IEEE Access
Multidisciplinary | Rapid Review | Open Access Journal

Received July 27, 2018, accepted September 19, 2018, date of publication September 24, 2018, date of current version October 31, 2018.

Digital Object Identifier 10.1109/ACCESS.2018.2871959

Optimal Design of Magnetic Coupling Wireless Power Supply System for Monitoring Equipment

ZHONGYU DAI, (Student Member, IEEE), JUNHUA WANG, (Member, IEEE), YIDA LI, YUANJIAN HE, ZHIJIAN FANG, (Member, IEEE), AND HAOLI HOU, (Member, IEEE)
School of Electrical Engineering, Wuhan University, Wuhan, China

Corresponding author: Junhua Wang (junhuawang@whu.edu.cn)

This work was supported in part by the National Natural Science Foundation of China under Grant 51707138 and Grant 51507114 and in part by the National Key Research and Development Plan under Grant 2017YFB1201002.

ABSTRACT The wireless power transfer technology provides a new solution to the power supply of monitoring devices. By adding a magnetic core that redistributes magnetic circuit, the proportion of the magnetic flux for power transmission increases, which improves the transmission efficiency. Based on a typical wireless power transmission model, the relationships between the parameters of the magnetic coupling mechanism and the transmission efficiency, as well as the parameters and the structure of the magnetic core, are analyzed. Under the premise of maximizing the transmission efficiency, the magnetic core is further optimized and its optimal parameters are designed. Compared with the traditional magnetic coupling mechanism, the proposed magnetic coupling mechanism with optimized magnetic cores improves the transmission efficiency by about 10%. This method indicates a new direction for optimizing the magnetic coupling mechanism of the wireless power supply system for monitoring equipment, as it can be applied to other wirelessly charged devices.

INDEX TERMS Magnetic coupling mechanism, magnetic core, wireless power transmission, coil optimization.

I. INTRODUCTION

The advent of Internet of Things (IoT) has a significant impact on our lives and work [1], [2]. The development of IoT is based on big data, which can deduce people's living habits and social needs, to better serve people [3]–[5]. To get data, lots of monitoring devices, such as cameras, sensors and so on, are used. As the wide use of monitoring equipment, the power supply problems are becoming more and more prominent [6], [7]. Conventional power supply modes of monitoring equipment are wire-powered and battery-powered [8], [9]. Wire-powered supply requires complex circuit when monitoring devices are densely installed, and demands a lot of manpower and resources. Furthermore, there is great chance that short circuit, fire or other accidents will occur when electric wires are aging. When using battery-powered supply, maintenance works, such as inspecting the battery capacity, replacing the battery, *etc.*, must be performed because of the limited battery capacity. Besides, heavy metal elements of the damaged battery are harmful to the environment [10], [11].

A great number of researches has been carried out to solve the power supply problems of monitoring devices, which can be classified into two groups. One is self-powered supply, while the other is wireless power transfer [8], [12]–[15]. The vibration energy harvest technique is a widely studied way of self-power-supplied methods [12]. But it only can obtain microwatt power and microampere current. The application range of it is very limited, and it is only suitable for ultra-low power sensors. The energy harvest technique based on the current transformer (CT) has also been widely studied in recent years [8], [16]. Its acquired power can reach watt power, and meet power supply requirements of most monitoring devices. However, it requires an intense magnetic field and mainly used for supplying high voltage transmission line monitoring equipment [16], [17]. Otherwise, the size of the CT is large and the weight is heavy. The ultrasonic wireless power supply is a way that transmits power via ultrasonic [13]. A lot of power will lose in the air medium The transmission efficiency is low, and the transmission distance is limited. Inductive wireless power transfer is a rather

popular technology [14], [18], and its transmission power ranges from milliwatt to kilowatt. However, the transmission efficiency will drop sharply when it exceeds a certain transmission distance. It is not suitable for long-distance power supply of monitoring devices. Based on the induction wireless power transfer technology, the resonant magnetic coupling wireless power transfer is proposed [15], [19], [20]. It uses compensation capacitors to adjust the resonance frequency of transmitters and receivers. This method can improve the transmission distance and the transmission efficiency. The transmission distance can reach 2 meters, which makes it best suitable for the power supply of monitoring devices.

The key part that determines transmission distance and efficiency is the magnetic coupling mechanism. There are two categories of coils composing the magnetic coupling mechanisms. The spiral coils are mainly used for short-distance and high-power power transmission, while the helix coils are used for long-distance and low-power transmission [15], [20]–[25]. The helix coils are more suitable for the power supply of monitoring devices. To improve the transmission distance and efficiency, many methods are used, such as relay coils, superconducting materials [15], [21], [26], [27]. However, the best way of adding magnetic cores to optimize the performance is seldom used in helix coils, as opposed to the spiral coils [19], [28].

The magnetic core can aggregate the magnetic field, reduce the leakage and increase the proportion of the magnetic flux for power transmission. In this paper, based on the idea that adding magnetic cores in the spiral coil to optimize the transmission distance and efficiency, the helix coil is optimized by adding magnetic cores [29]. To reduce the loss of magnetic flux in the air, the characteristics of the magnetic circuit is considered, and a unique-shaped core is designed to guide the magnetic flux. It can effectively improve the transmission distance and efficiency.

II. TRANSMISSION EFFICIENCY

Fig. 1. shows the equivalent circuit of the typical wireless power transfer system. The power is converted to high-frequency AC power through rectification and inversion, and then transmitted from the transmitting coil to the receiving coil through the electromagnetic field. Through rectification, the AC power of the receiving coil is converted to DC power

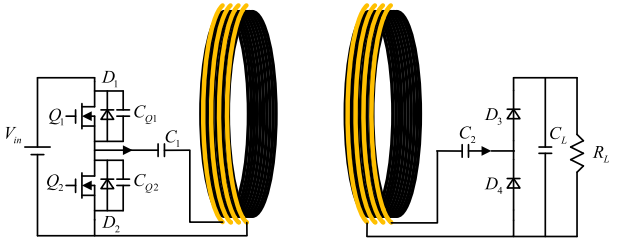

FIGURE 1. The topology of wireless power transfer system.

to supply monitoring devices. To improve the transmission efficiency and distance, the transmitting coil and the receiving coil require series or parallel compensating capacitor to ensure that both of the circuits own the same resonant frequency.

The inverter and rectifier are neglected to simplify the analysis process, as shown in Fig. 2. L_1 and L_2 are self-inductance of the transmitting coil and the receiving coil respectively. M is the mutual inductance. R_1 and R_2 are the AC resistance of transmitting coil and receiving coil, and U_s is the sinusoidal voltage source with a frequency of f. Based on KVL, we have

$$\begin{bmatrix} U_S \\ 0 \end{bmatrix} = \begin{bmatrix} R_1 + j\omega L_1 + 1/j\omega C_1 & j\omega M \\ j\omega M & R_L + R_2 + j\omega L_2 + 1/j\omega C_2 \end{bmatrix} \times \begin{bmatrix} I_1 \\ I_2 \end{bmatrix}. \quad (1)$$

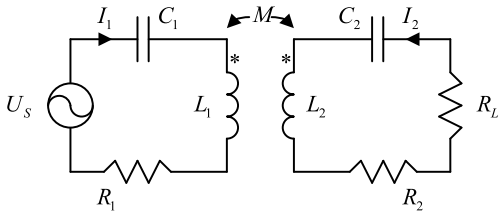

FIGURE 2. The equivalent circuit of a simplified wireless power transfer system.

When the transmitting coil and the receiving coil have the same resonant frequency, we have $j\omega L_1 + 1/j\omega C_1 = 0$ and $j\omega L_2 + 1/j\omega C_2 = 0$. The transmission efficiency is

$$\eta = \frac{\alpha k^2 Q_1 Q_2}{(1+\alpha)^2 + (1+\alpha) k^2 Q_1 Q_2}. \quad (2)$$

Where $\alpha = R_L/R_2$ is the load factor, $k = M/\sqrt{L_1 L_2}$ is the coupling coefficient. $Q_1 = \omega L_1/R_1$ and $Q_2 = \omega L_2/R_2$ are the quality factors of the transmitting coil and the receiving coil.

The wireless power transfer system is in a weak coupling state when it supplies power for monitoring devices. The current of the receiving coil is very small. When it is launched to the transmitting coil through very low mutual inductance, it can be ignored [23], [24]. Therefore, equation (2) can be simplified into

$$\eta = \frac{\alpha}{(1+\alpha)^2} k^2 Q_1 Q_2. \quad (3)$$

From equation (3), the transmission efficiency is positively related to the quality factors of the transmitting coil and the receiving coil, and it is also positively related to the square of the coupling coefficient. To improve the transmission efficiency, the quality factor and coupling coefficient of the coils should be optimized. In addition, the resonant frequency is *kHz*. The high-frequency characteristics of the coils are non-negligible.

A. THE INDUCTANCE

The definition of self-inductance is the ratio of the inter-linkage magnetic flux of the loop current and the circuit current producing magnetic flux [20], [24], [30]. For a single turn circular coil, it can be expressed as

$$L_S = \mu_0 R\left[\ln\left(\frac{8R}{r}\right) - 2\right] \tag{4}$$

Where μ_0 is the permeability of vacuum, R is the radius of the single turn coil, r is the radius of the wire.

The mutual inductance is defined as the ratio of the mutual flux to the loop of any coil and the circuit current that produces secondary mutual flux. For two parallel single-turn loop coils, the following equation can be obtained according to [20] and [22].

$$M = \mu_0\pi\sqrt{R_1R_2}\int_0^{\infty} J_1\left(x\sqrt{\frac{R_1}{R_2}}\right)J_1\left(x\sqrt{\frac{R_2}{R_1}}\right) \times J_0\left(x\frac{L}{\sqrt{R_1R_2}}\right)\exp\left(-x\frac{D}{\sqrt{R_1R_2}}\right)dx \tag{5}$$

Where R_1 and R_2 are the radius of the single-turn transmitting coil and receiving coil, D is the distance between the two coils, L is the lateral offset distance of the two coils, J_0 and J_1 are the Bessel functions of the zeroth and first order [31].

The transmitting coil and the receiving coil are usually single-layer multi-turn coils. The self-inductances of the coils include the inductance of all the single-turn coils and the mutual inductance between the single-turn coils. Hence the self-inductance of the single layer N-turn coils can be expressed as

$$L = \sum_{i=1}^{N}\sum_{j=1}^{N} M\left(R, R, L = 0, D_{ij} = |j - i|\, d'\right)\left(1 - \kappa_{ij}\right) + \sum_{1}^{N} L_S\left(R, r\right). \tag{6}$$

Where d' is the distance between two adjacent single-turn coils, κ_{ij}= 1 when $i = j$, otherwise, κ_{ij}= 0.

Assume the transmitting coil and the receiving coil are supposed to have the same turns. To achieve the best transmission efficiency, the transmitting coil and the receiving coil must remain coaxial, which means the lateral offset L= 0. The mutual inductance between the two coils is

$$M_{ab} = \sum_{i=1}^{N}\sum_{j=1}^{N} M\left(R, R, L = 0, D_{ij} = (N + j - i)\, d' + d\right) \tag{7}$$

Where d is the closest distance between the transmitting coil and the receiving coil.

From above equations, the coupling factor between the transmitting coil and receiving coils can be obtained as (8), shown at the bottom of this page.

B. THE PARASITIC CAPACITANCE

The parasitic capacitances exist between the single-turn coils. They have a significant influence on the resonant frequency and the transmission efficiency. For the coil with a shielding layer, there is also a parasitic capacitance between the single-turn coil and the shielding. According to the equivalent circuit of parasitic capacitance [32], as shown in Fig. 3, the total parasitic capacitance can be calculated as

$$C_{(N)} = \frac{C_{(N-2)} \cdot C_1}{2C_{(N-2)} + C_1} + \frac{C_2}{2} \tag{9}$$

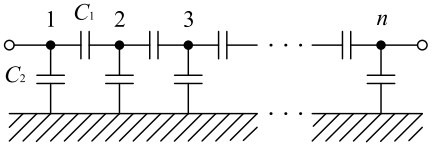

FIGURE 3. The equivalent circuit of parasitic capacitance.

Where N is the turns of the coil, which requires that $N > 3$. When $N = 1$, there is no parasitic capacitance. When $N = 2$, $C_{(2)} = C_1 + C_2/2$. When $N = 3$, $C_{(2)} = C_1/2 + C_2/2$. Where C_1 is the capacitance between single-turn coils, C_2 is the capacitance between the single-turn coil and the shielding layer.

For a helix coil with a shield layer, the parasitic capacitances between the single-turn coils and the parasitic capacitances between the single-turn coils and a shielding layer are

$$C_1 = \frac{2\pi^2 R\varepsilon_0}{\ln\left(d'/2r + \sqrt{(d'/2r)^2 - 1}\right)} \tag{10}$$

$$C_2 = \frac{4\pi^2 R\varepsilon_0}{\ln\left(h/r + \sqrt{(h/r)^2 - 1}\right)} \tag{11}$$

Where R is the coil radius, d' is the winding pitch, r is the wire radius, h is the distance from the coils to the shielding layer.

Fig. 4 shows the variations of parasitic capacitance with the pitch between the single-turn coil and the distance between the single-turn coil and the shielding. The parasitic capacitances have the same change law in either of these cases.

$$k = \frac{\sum_{i=1}^{N}\sum_{j=1}^{N} M\left(R, R, L = 0, D_{ij} = (N + j - i)\, d' + d\right)}{\sum_{i=1}^{N}\sum_{j=1}^{N} M\left(R, R, L = 0, D_{ij} = |j - i|\, d'\right)\left(1 - \kappa_{ij}\right) + \sum_{1}^{N} L_S\left(R, r\right)} \tag{8}$$

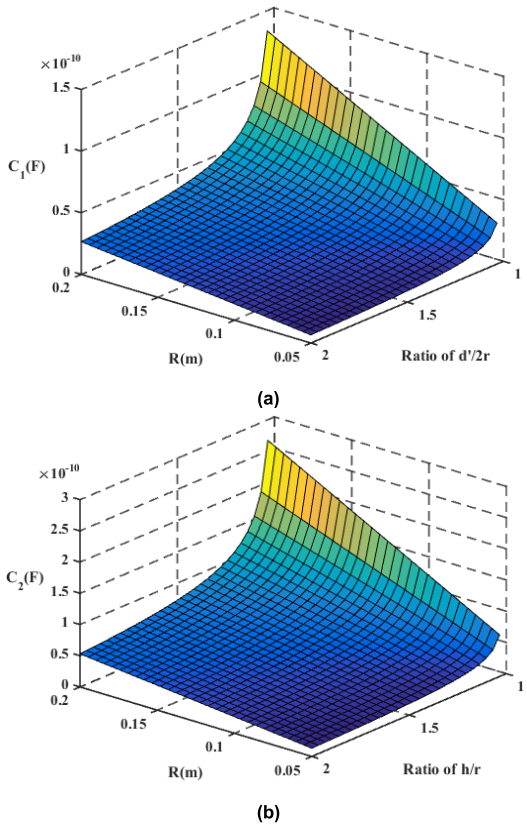

FIGURE 4. The parasitic capacitances. (a) The parasitic capacitance varies with pitch. (b) The parasitic capacitance varies with the distance of shielding structure.

There is a positive correlation between the parasitic capacitances and the radius of the single-turn coils, while a negative correlation with the ratio of $d^{'}/2r$ and h/r.

C. THE AC IMPEDANCE

When the transmitting and receiving coils operate at a low frequency or in the DC state, the resistance of the coils is almost invariable [20], which is called the DC resistance. The DC resistance of a single-layer N-turn coil is

$$R_{DC} = \rho \cdot \frac{2NR}{r^2} = 2N\pi RR_0 \tag{12}$$

Where ρ is the resistivity, R_0 is the resistance per unit length of wire.

The normal operating frequency of the wireless power transfer system is above *kHz*. At such frequency, there are skin effect and proximity effect in the wire. The AC resistance is

$$R_{AC} = R_{DC}\left(1 + \frac{f^2}{f'^2}\right) \tag{13}$$

Where f' is the frequency at which power dissipation is twice of the DC power dissipation and is given by [20], [33]

$$f' = \frac{2\sqrt{2}}{\pi r^3 \mu_0 \sigma \sqrt{N\eta_R \beta}} \tag{14}$$

Where σ is the conductivity, η_R is area efficiency of coil with width b and thickness t and can be calculated using Fig. 5. β is the area efficiency defined as the ratio of the total conducting area over the cross section of the winding [26].

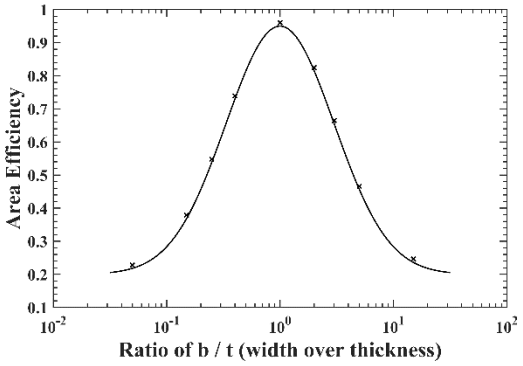

FIGURE 5. β versus coil aspect ratio (b/t).

D. THE QUALITY FACTOR

When the wireless power transfer system operates at *kHz* level, with the effect of the parasitic capacitance and the AC resistance, the total impedance of the coil is

$$\begin{aligned} Z &= (j\omega L + R_{AC}) \,||\, \frac{1}{j\omega C} \\ &= \frac{R_{AC} + j\omega\left[L\left(\omega^2 LC - 1\right) - CR^2\right]}{\omega^2 C^2 R_{AC}^2 + \left(1 - \omega^2 LC\right)^2} \end{aligned} \tag{15}$$

From equation (15), the impedance can be simplified as the series structure of the equivalent resistance R_{eq} and the equivalent inductor L_{eq}. The coil resistance can be ignored when compared with the reactance, and we have

$$R_{eq} = \frac{R_{AC}}{\left(1 - \omega^2 LC\right)^2} \tag{16}$$

$$L_{eq} = \frac{L}{1 - \omega^2 LC}. \tag{17}$$

Therefore, the quality factor of the coil is

$$Q = \frac{\omega L_{eq}}{R_{eq}} = \frac{2\pi fL\left(1 - f^2/f_{LC}^2\right)}{R_{DC}\left(1 + f^2/f'^2\right)} \tag{18}$$

Where $f_{LC} = 1/2\pi\sqrt{LC}$ is the resonance frequency without compensation of the coil.

Fig. 6. shows the relationships among the quality factor Q, the inductance and the parasitic capacitance of the coil. Obviously, the Q is increasing with the increase of the inductance and the decrease of the parasitic capacitance. When the parasitic capacitance is relatively large, the quality factor increases first and then decreases with the increase of inductance.

III. THE OPTIMIZATION MAGNETIC CORE

From equations (6) and (18), the quality factor of the coil is related to the permeability of the coil. To improve the quality

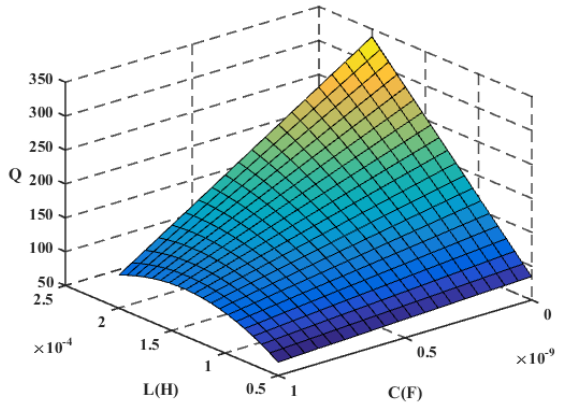

FIGURE 6. The relationships among the quality factor Q, the inductance and the parasitic capacitance of the coil.

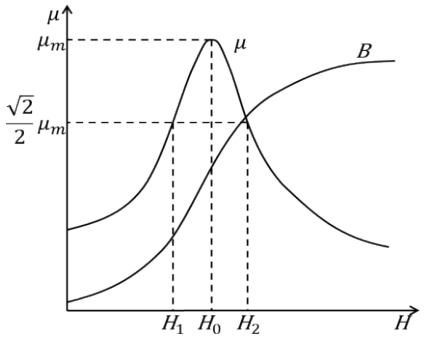

FIGURE 7. The magnetic permeability curve.

factor, adding a toroidal core in the center of the helix coil, as shown in Fig. 1.

The magnetic permeability curve of the core is shown in Fig. 7. [27]. The magnetic induction intensity increases with the increase of magnetic field strength. The permeability first increases then decreases. The coil inductance reaches the maximum when the permeability reached its summit. To use magnetic core material efficiently and economically, assume that the magnetic permeability is in the range of $\sqrt{2}/2\mu_m$ and $1\mu_m$ when the magnetic core material is in normal operation state. It means that the magnetic core is installed in the area with the magnetic field intensity ranging from H_1 to H_2.

The size, turn number and operating current of the coil can be determined after the wireless power transfer system is designed. According to the Ampere loop law [28], we have

$$\oint_l H \cdot dl = \sum I. \tag{19}$$

The magnetic field intensity at a distance r from the center of a single-turn coil can be expressed as $H = I/2\pi(R - r_n)$, which is shown in Fig. 8.

In Fig. 8, R is the radius of the coil. r_1 and r_2 are the distance from the center of the coil to the inner and outer side of the magnetic core. r_0 is distance from the center of the coil to the point where the magnetic induction intensity is H_0,

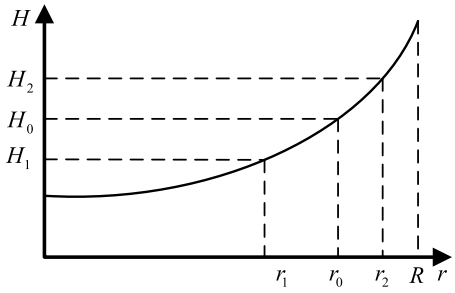

FIGURE 8. H versus r.

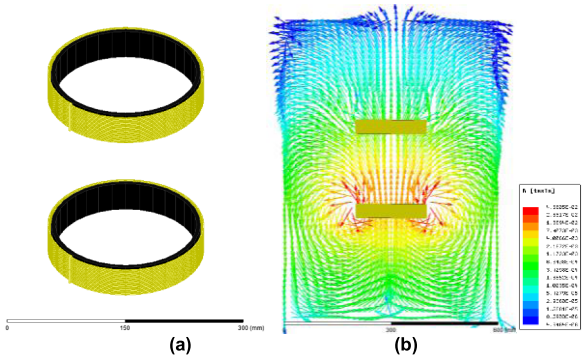

FIGURE 9. Electromagnetic simulation analysis. (a) The simulation model. (b) The magnetic field vector.

that is where the magnetic permeability is *1* μ_m. To reduce the weight of the magnetic coupling mechanism and for the convenience of the physical design, the magnetic core parameters is simplified to meet r_2-$r_0 = r_0$-r_1. Consequently, the magnetic core is installed at the distance r_0 from the center of the coil, and the thickness of it is $D = 2(r_2$-$r_0)$.

To simplify the analysis, the transmitting coil and the receiving coil are the same structure. Then, the models of the coils and magnetic cores are built, and solved at a frequency of 150kHz, as shown in Fig. 9(a). Fig. 9(b). shows the nephogram of the magnetic field vector.

The magnetic field is a passive field, and all lines of magnetic induction must constitute closed loops. From Fig. 9(b)., because the permeability of the core is much larger than that of the air, the magnetic induction lines is mainly concentrated in the magnetic core, and then passes through the outer area of the coil to form closed loops. In the magnetic core, due

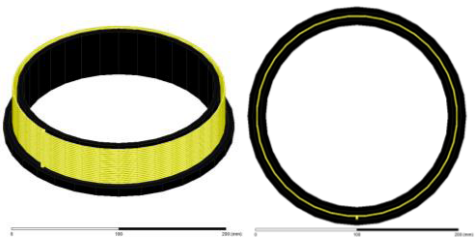

FIGURE 10. The optimized magnetic core structure.

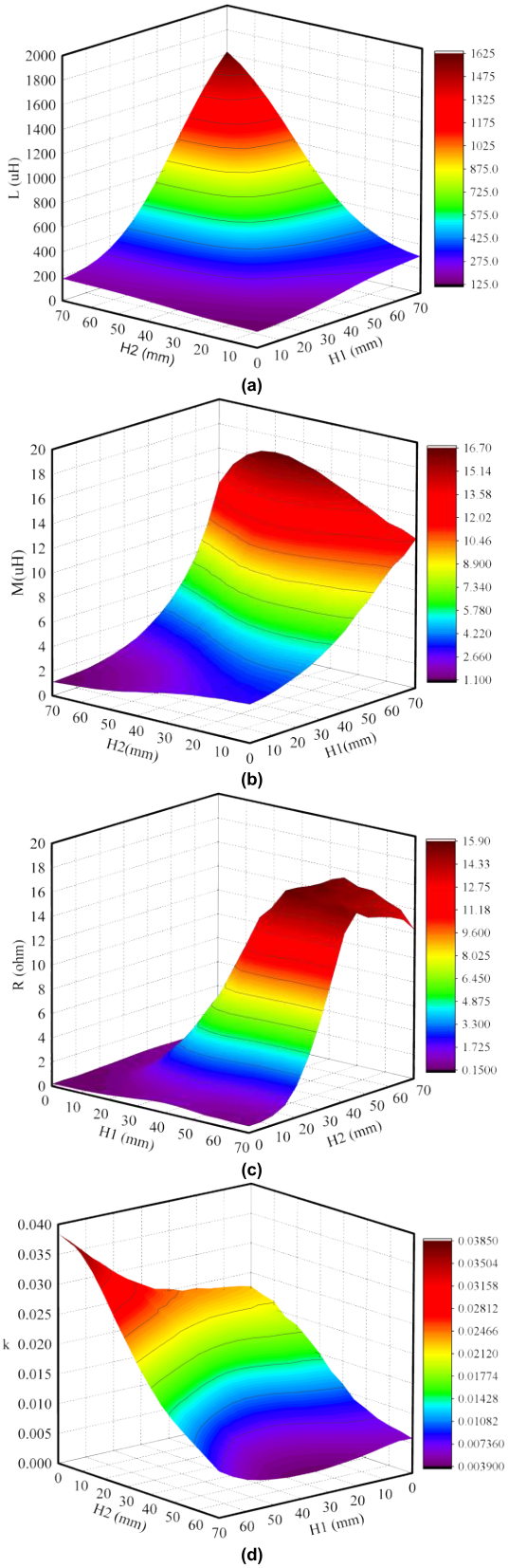

FIGURE 11. The variation of coil parameters with the changes of the height of inner and outer magnetic cores. (a) The self-inductance. (b) The mutual-inductance. (c) The resistance. (d) The coupling factor.

to its constraint, the magnetic induction lines are along the direction of the magnetic core. However, there is no guidance of the magnetic core at the outer and the edge of the coil, the magnetic induction line is long and highly jumbled.

To shorten the path of magnetic induction lines and reduce the loss of magnetic field in air, the magnetic core is optimized. As shown in Fig. 10., a hook-shaped magnetic field guide is added at the edge of the coil.

To further investigate the influence of the inner and outer magnetic cores, the corresponding models are established and the parameter scanning analysis is conducted. The results are shown in Fig. 11., where H_1 is the height of outer magnetic core and H_2 is the height of inner.

Fig. 11. shows the influence of the magnetic core parameters on the magnetic coupling mechanism, including self-inductance, mutual-inductance, resistance and coupling factor. From Fig. 11(a)., with the increase of the height of the inner and outer magnetic core, the self-inductance of the coil increases, and the height of the outer magnetic core has a greater influence. The mutual inductance increases continuously when the height of the outer magnetic core increases shown in Fig. 11(b)., and it increases firstly and then decreases with the change of the inner magnetic core. According Fig. 11(c)., as the height of inner and outer magnetic cores increases, the resistance goes up first but then it goes down. It reaches the maximum when the height of the inner is about 50mm. The coupling coefficient is shown in Fig. 11(d). It is on a downward trend as the raise of the height of the inner magnetic core. With the change of the outer magnetic core, it presents a down and up trend.

According to the equation (18), the quality factor of the coil can be calculated as shown in Fig. 12. It rises first and descends later with the increase of the inner magnetic core height, and attains the maximum when the inner magnetic is about the same height as the coil. As the change of the outer, it shows downward trend. It is easy to find the quality factor

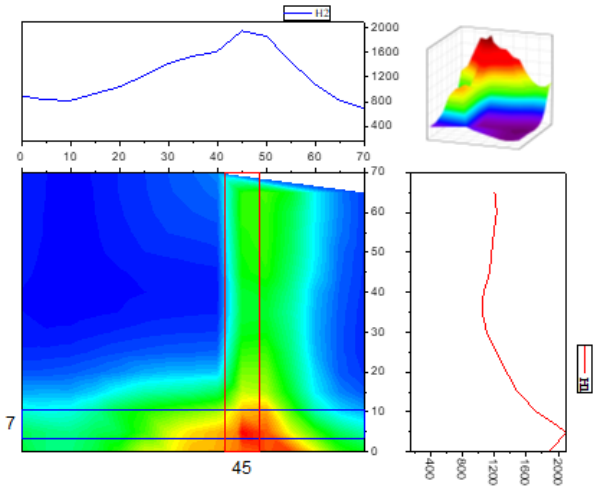

FIGURE 12. The quality factor.

reaches the maximum when the height of the outer magnetic core is about *7mm* and the inner is about *45mm*.

IV. THE DESIGN OF THE MAGNETIC COUPLING MECHANISM

Based on above analyses, a model of the magnetic coupling mechanism of the wireless power transfer system for monitoring devices is designed, as shown in Fig. 13, which includes:

1) the helix coil
2) the optimized magnetic core

FIGURE 13. The magnetic coupling part model of wireless power transfer system for monitoring devices. (a) The coil. (b) The optimized magnetic core structure.

A. THE HELIX COIL

The physical model of the Helix coil is shown in Fig. 13(a). To achieve a farther transmission distance, the radius of the coil should be as large as possible. However, the larger the radius is, the more material and space will be required. By considering the transmission distance and the volume of the devices, the radius of the coil is determined to be *100mm*. From the equation (6), the inductance of the coil is proportional to the square of its turns, and the coil turns is determined as *20* turns. The specific coil parameters are shown in Table 1.

TABLE 1. The coil parameters.

Parameter	Value
wire material	enameled wire
coil radius	*100mm*
wire radius	*1mm*
wire pitch	*2.2mm*
turns	*20*
self-inductance	*125.5uH*

B. THE OPTIMIZED MAGNETIC CORE

The TDK's MnZn ferrite is chosen to be the magnetic core material [34]. Under normal operation condition, the total current of the coil *NI* is about *3A*. According to Fig. 7, Fig. 8 and equation (19), when the magnetic permeability is $\sqrt{2}/2\mu_m$, H_1 and H_2 are *12.71A/m* and *37.13A/m*. H_0 is *30.24A/m* when $\mu = 1\mu_m$. R and r are 100mm and 1mm that known from Table 1. It can be seen that the section of the coil is similar to a rectangle from Fig. 14. So the path in the Ampere's law is modified from the $2\pi(R\text{-}r_n)$

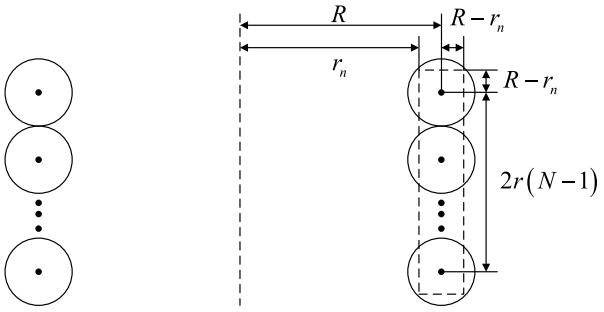

FIGURE 14. The section of the coil.

to $2[2r(N\text{-}1)+2(R\text{-}r_n)+2(R\text{-}r_n)]$. That is $H = NI/2[2r(N\text{-}1)+2(R\text{-}r_n)+2(R\text{-}r_n)]$. Then r_1, r_2, and r_0 are be calculated, which are *80.0mm*, *99.4mm* and *97.1mm*, respectively. So the thickness of the magnetic core is $D = 2(r_2\text{-}r_0) = 4.6mm$. Because $R\text{-}r_2 = 0.6mm$ is less than the radius r of the wire, and the magnetic core cannot be installed inside the wire, the r_2 is modified from *99.4mm* to *99mm*. That is the magnetic core is installed next to the coil not inside. Therefore, the MnZn ferrite with common $5 \times 15 \times 50mm$ size is used to manufacture the magnetic core. To achieve higher transmission efficiency, the coupling coefficient and quality factor of the coil should be as high as possible. By combining Fig. 11, Fig. 12. and equation (3), the heights of the inner core and the outer core are set to *45mm* and *7mm* respectively. The physical core structure is shown in Fig. 13(b).

V. EXPERIMENT

Based on the design of the magnetic coupling mechanism, a corresponding experimental platform is built, as shown in Fig. 15. The resonant frequency of the magnetic coupling mechanism with or without a magnetic core is matched to 150kHz by compensation capacitors.

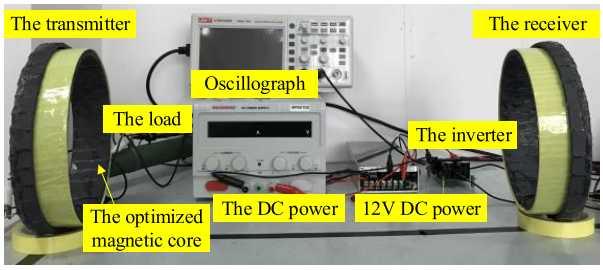

FIGURE 15. The experiment platform.

Transmission efficiencies of the magnetic coupling mechanism with or without optimized cores are compared as shown in Fig. 16. It can be obtained that, when the input power increases from *0W* to *2W*, the transmission efficiency of the system keeps increasing, but the increasing rate is decreasing. After the input power reaches *2W*, the transmission efficiency is stable. The transmission efficiency of magnetic coupling mechanism with an optimized magnetic core is about *10%* higher than that without magnetic core at a distance of *45cm*.

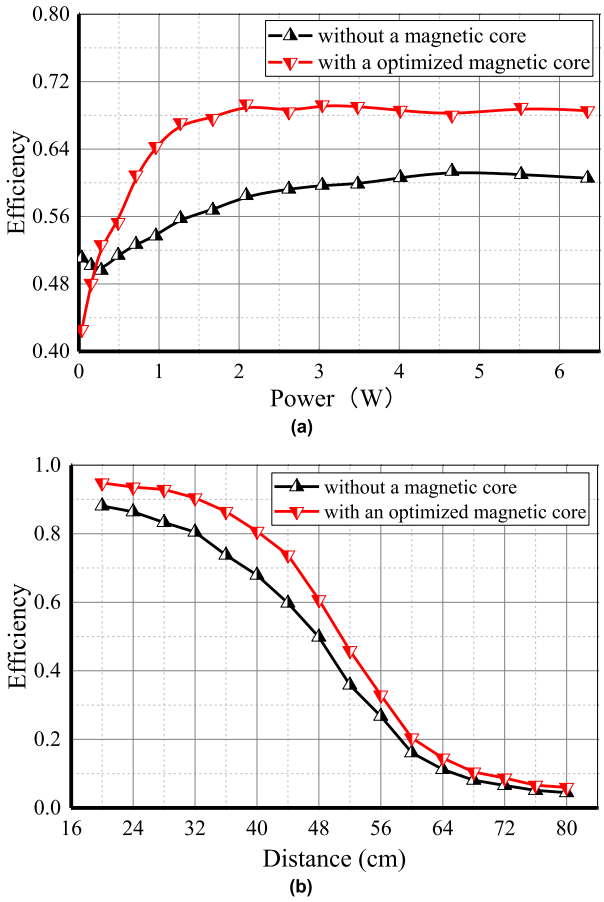

FIGURE 16. **The transmission efficiency of the magnetic coupling part. (a) Distance of 45cm. (b) Power of 5W.**

Because when the input power is small, the loss of the system accounts for a large proportion of the total power. When the input power increases continuously, the proportion of this part of the loss keep decreasing until it becomes stable. At this time, the transmission efficiency can remain relatively stable. In Fig. 16(b), with the increase of distance, the transmission efficiencies of the magnetic coupling mechanism with or without optimized cores gradually decrease. And the transmission efficiency of the one without magnetic core is lower than that with an optimized magnetic core throughout the experiments. In the range of *40cm* to *60cm*, the transmission efficiencies decrease sharply with the increase of distance. When the distance reaches *60cm*, the transmission efficiencies are below *20%*. Based on the comparison, the optimized magnetic coupling mechanism can effectively improve the transmission efficiency and the distance of the magnetic coupling wireless power supply system for monitoring equipment.

VI. CONCLUSION

In this paper, the magnetic coupling mechanism of the wireless power transfer system with an optimized magnetic core is proposed. Based on a typical wireless power transfer system, the key parameters of the magnetic coupling mechanism are analyzed, including the inductance, the parasitic capacitance, the AC/DC resistance, the coupling coefficient and the quality factor. The influences of the magnetic core parameters are analyzed, and the parameters of the optimal core structure (the heights of the inner core and the outer core are set to *45mm* and *7mm* respectively) are designed. The experiment results show the magnetic coupling mechanism with an optimized magnetic core improves the transmission efficiency by about *10%*. The proposed optimized scheme is also suitable for the optimization of the wireless power supply system of other devices, especially some devices that require longer power transmission distance.

REFERENCES

[1] Q. Zhang, L. T. Yang, Z. Chen, and P. Li, "High-order possibilistic c-means algorithms based on tensor decompositions for big data in IoT," *Inf. Fusion*, vol. 39, pp. 72–80, Jan. 2018.
[2] S. Neethirajan, S. K. Tuteja, S.-T. Huang, and D. Kelton, "Recent advancement in biosensors technology for animal and livestock health management," *Biosensors Bioelectron.*, vol. 98, pp. 398–407, Dec. 2017.
[3] F. Firouzi *et al.*, "Internet-of-Things and big data for smarter healthcare: From device to architecture, applications and analytics," *Future Gener. Comput. Syst.*, vol. 78, pp. 583–586, Jan. 2018.
[4] M. Abu Alsheikh, D. Niyato, S. Lin, and H.-P. Tan, and Z. Han, "Mobile big data analytics using deep learning and apache spark," *IEEE Netw.*, vol. 30, no. 3, pp. 22–29, May/Jun. 2016.
[5] Z. Yan, "Big data fusion in Internet of Things," *Inf. Fusion*, 2017.
[6] I. M. Moreno-Garcia *et al.*, "Real-time monitoring system for a utility-scale photovoltaic power plant," *Sensors*, vol. 16, no. 6, p. 770, 2016.
[7] Z. Chen, X. Chen, D. Zhang, and F. Zeng, "Collaborative mobile charging policy for perpetual operation in large-scale wireless rechargeable sensor networks," *Neurocomputing*, vol. 270, pp. 137–144, Dec. 2017.
[8] L. Xiong, Y.-Z. He, D.-J. Song, Y. Liu, W. He, and Z.-L. Zhang, "Design on power supply for the transmission line on-line monitoring equipment," *High Voltage Eng.*, vol. 36, no. 9, pp. 2252–2257, 2010.
[9] Z. Dai, Z. Fang, H. Huang, Y. He, and J. Wang, "Selective omnidirectional magnetic resonant coupling wireless power transfer with multiple-receiver system," *IEEE Access*, vol. 6, pp. 19287–19294, 2018.
[10] R. D. Collier and K. Kaliski, "A low-complexity environmental noise monitoring system for unattended operation in remote locations," *J. Acoust. Soc. Amer.*, vol. 121, no. 5, p. 3160, 2007.
[11] J. W. Stockdale, "Battery powered gaming machine security monitoring system," U.S. Patent 6 575 833 B1, Jun. 10, 2003.
[12] S. R. Anton and H. A. Sodano, "A review of power harvesting using piezoelectric materials (2003–2006)," *Smart Mater. Struct.*, vol. 16, no. 3, p. R1, 2007.
[13] L. H. Fai and A. P. Hu, "Modeling and analysis of ultrasonic power transfer system with tightly coupled solid medium," *Wireless Power Transfer*, vol. 4, no. 1, pp. 1–12, 2016.
[14] Z. N. Low, R. A. Chinga, R. Tseng, and J. Lin, "Design and test of a high-power high-efficiency loosely coupled planar wireless power transfer system," *IEEE Trans. Ind. Electron.*, vol. 56, no. 5, pp. 1801–1812, May 2009.
[15] X. Liu and G. Wang, "A novel wireless power transfer system with double intermediate resonant coils," *IEEE Trans. Ind. Electron.*, vol. 63, no. 4, pp. 2174–2180, Apr. 2016.
[16] W. Li, X. Fu, Y. Bai, and G. Wu, "Development of power induction devices for transmission lines," *Eng. J. Wuhan Univ.*, vol. 44, no. 4, pp. 516–520, Jul. 2011.
[17] W. Wang, X. Huang, L. Tan, J. Guo, and H. Liu, "Optimization design of an inductive energy harvesting device for wireless power supply system overhead high-voltage power lines," *Energies*, vol. 9, no. 4, p. 242, 2016.
[18] P. S. Yedavalli, T. Riihonen, X. Wang, and J. M. Rabaey, "Far-field RF wireless power transfer with blind adaptive beamforming for Internet of Things devices," *IEEE Access*, vol. 5, pp. 1743–1752, 2017.
[19] Z. Dai, J. Wang, M. Long, H. Huang, and M. Sun, "Magnetic shielding structure optimization design for wireless power transmission coil," *Aip Adv.*, vol. 7, no. 9, p. 095013, 2017.

[20] A. K. Ram Rakhyani, S. Mirabbasi, and M. Chiao, "Design and optimization of resonance-based efficient wireless power delivery systems for biomedical implants," *IEEE Trans. Biomed. Circuits Syst.*, vol. 5, no. 1, pp. 48–63, Feb. 2011.
[21] E. S. G. Rodríguez, A. K. RamRakhyani, D. Schurig, and G. Lazzi, "Compact low-frequency metamaterial design for wireless power transfer efficiency enhancement," *IEEE Trans. Microw. Theory Techn.*, vol. 64, no. 5, pp. 1644–1654, May 2016.
[22] P. J. Abatti, C. M. de Miranda, M. A. P. da Silva, and S. F. Pichorim, "Analysis and optimisation of three-coil wireless power transfer systems," *IET Power Electron.*, vol. 11, no. 1, pp. 68–72, Dec. 2018.
[23] M. R. Basar, M. Y. Ahmadm, J. Cho, and F. Ibrahim, "Stable and high-efficiency wireless power transfer system for robotic capsule using a modified helmholtz coil," *IEEE Trans. Ind. Electron.*, vol. 64, no. 2, pp. 1113–1122, Feb. 2017.
[24] C. Zhang and Y. Chen, "Wireless power transfer strategies for cooperative relay system to maximize information throughput," *IEEE Access*, vol. 5, pp. 2573–2582, 2017.
[25] Z. Dai, J. Wang, M. Long, and H. Huang, "A witricity-based high-power device for wireless charging of electric vehicles," *Energies*, vol. 10, no. 3, p. 323, 2017.
[26] J. Lee, K. Lee, and D.-H. Cho, "Stability improvement of transmission efficiency based on a relay resonator in a wireless power transfer system," *IEEE Trans. Power Electron.*, vol. 32, no. 5, pp. 3297–3300, May 2017.
[27] Y. Do Chung, C. Y. Lee, H. Kang, and Y. G. Park, "Design considerations of superconducting wireless power transfer for electric vehicle at different inserted resonators," *IEEE Trans. Appl. Supercond.*, vol. 26, no. 4, Jun. 2016, Art. no. 0603605.
[28] J. Kim *et al.*, "Coil design and shielding methods for a magnetic resonant wireless power transfer system," *Proc. IEEE*, vol. 101, no. 6, pp. 1332–1342, Jun. 2013.
[29] X. Xin, D. R. Jackson, and J. Chen, "Wireless power transfer along oil pipe using ferrite materials," *IEEE Trans. Magn.*, vol. 53, no. 3, Mar. 2017, Art. no. 9200205.
[30] K. R. Demarest, "Engineering electromagnetics," *IEEE Elect. Insul. Mag.*, vol. 15, no. 3, p. 51, 2006.
[31] C. M. Zierhofer and E. S. Hochmair, "Geometric approach for coupling enhancement of magnetically coupled coils," *IEEE Trans. Biomed. Eng.*, vol. 43, no. 7, pp. 708–714, Jul. 1996.
[32] G. Grandi, M. K. Kazimierczuk, A. Massarini, and U. Reggiani, "Stray capacitances of single-layer solenoid air-core inductors," *IEEE Trans. Ind. Appl.*, vol. 35, no. 5, pp. 1162–1168, Sep./Oct. 1999.
[33] Z. Yang, W. Liu, and E. Basham, "Inductor modeling in wireless links for implantable electronics," *IEEE Trans. Magn.*, vol. 43, no. 10, pp. 3851–3860, Oct. 2007.
[34] H. Aiping and P. Loss, "Permeability and impedance characteristics and preparation technology of manganese zinc ferrites," Ph.D. dissertation, Huazhong Univ. Sci. Technol., Wuhan, China, 2006.

ZHONGYU DAI received the B.Sc. degree from Wuhan University, where he is currently pursuing the Ph.D. degree. His main research interests include wireless transmission technology based on magnetic resonance, applied electromagnetics, and system equipment for power transmission and distribution.

JUNHUA WANG was born in Shandong, China, in 1981. He received the Ph.D. degree from The Hong Kong Polytechnic University, Hong Kong, in 2012. He joined Carnegie Mellon University as a Post-Doctoral Researcher in 2012, and then he was a Research Fellow at the GATE Center for Electric Drive Transportation, MI, USA. He is currently a Professor with the School of Electrical Engineering, Wuhan University. His main research interests include wireless transmission technology based on magnetic resonance, applied electromagnetics, and system equipment for power transmission and distribution.

YIDA LI received the B.Eng. degree from Wuhan University in 2016, where he is currently pursuing the master's degree. His main research interests include power electronic, battery management systems.

YUANJIAN HE received the bachelor's degree from North China Electric Power University in 2015. He is currently pursuing the M.E.E. degree with Wuhan University. His main research interest covers the wireless transmission technology based on magnetic resonance, power electronics, and applied electromagnetics.

ZHIJIAN FANG received the B.S. and Ph.D. degrees in electrical engineering and automation from the Huazhong University of Science and Technology, Wuhan, China, in 2010 and 2015, respectively.

Since 2015, he has been a Post-Doctoral Research Fellow with the School of Electrical Engineering, Wuhan University, Wuhan. From 2016 to 2017, he was a Post-Doctoral Research Fellow with the Department of Electrical and Computer Engineering, Ryerson University, Toronto, Canada. His research interests include high-performance dc/dc converters, battery chargers, and renewable energy applications.

HAOLI HOU received the Ph.D. degree in genetics from the College of Life Sciences, Wuhan University, Wuhan, China, in 2017. Since 2017, she has been a Post-Doctoral Research Fellow with the School of Electrical Engineering, Wuhan University, Wuhan. Her main research area is molecular cytogenetics, biological effect of high-frequency magnetic field, effect of low temperature on plasma, and other related research topics.